Journal of Applied Fluid Mechanics, Vol. 9, No. 3, pp. 1339-1348, 2016.
Available online at www.jafmonline.net, ISSN 1735-3572, EISSN 1735-3645.
DOI: 10.18869/acadpub.jafm.68.228.24612

Simulation of Flow and Heat Transfer of Mist/Air Impinging Jet on Grinding Work-Piece

F. Jiang [1†], H. Wang [2], Y. Wang [1] and J. Xiang [1]

1. School of Mechanical and Electric Engineering, Guangzhou University, Guangzhou, 510006, China
2. School of Electro-mechanical Engineering, Guangdong University of Technology, Guangzhou, 510006, China

†Corresponding Author Email: jiangfan2008@gzhu.edu.cn

(Received January 26, 2015; accepted July 19, 2015)

ABSTRACT

The numerical investigation is presented for flow and heat transfer on grinding work-piece with mist/air impinging jet by using DPM (discrete phase model) model. The tracks of the mist droplets show most of them are accumulated on the right surface of grinding zone, and can be influenced by the rotating speed of the grinding wheel, the position and the number of the jet nozzle. The mechanism model of enhance cooling by mist/air impinging jet is developed, which indicated the mist droplet is an key factor of affecting the heat transfer coefficient, and the increasing of mist droplet leads to significant enhancement of the cooling effect. The effects of the jet nozzle location, the nozzle diameter, and the nozzle number on flow and heat transfer coefficient are studied. The results show that the less nozzle distance and inclination angle, the greater nozzle diameter and number lead to greater heat transfer coefficient.

Keywords: Mist/air impinging jet; Heat transfer; DPM; Mist droplets trajectory; Numerical simulation; Grinding zone cooling.

NOMENCLATURE

A	effective area of heating foil
a_k	inverse effective Prandtl numbers for k
a_ε	the inverse effective Prandtl numbers for ε
$C_{1\varepsilon}, C_{2\varepsilon}, C_{31\varepsilon}$	turbulence model constants
d_p	is particle diameter
$\vec{F}_{c,i}$	particle-wall force
g	gravitational constant
G_k	the generation rate of turbulence kinetic energy
G_b	the generation rate of turbulence kinetic energy
h	local convective heat transfer coefficient
h_0	air alone heat transfer coefficient
I_i	moment of inertia of the mist particle
K	consistency index
k_s	air heat conductivity
p_a	air pressure in the flow field
Q	input power imposing on heating foil
Q_s	heat loss from heater insulation
Re	particle Reynolds number
t	time
$\vec{T}_i$	torque
T_k	thermal conductivity
T_w	heated plate temperature on the top surface
T_j	jet temperature
$\vec{v}_a$	velocity of the air phase
v_i	particle velocity
V_i	volume
ρ_a	air density
μ_a	dynamic viscosity of the air phase
μ_{eff}	effective viscosity
α	phase fraction
α_a	phase fraction of the air phase
η	interphase momentum transfer coefficient
γ	coefficient
$\vec{\tilde{\tau}}_a$	stress tensor for air phase
r_i	particle position
$\vec{S}_p$	drag force sink term
Δp	total pressure drop

1. INTRODUCTION

Grinding is widely concerned in the machining field, which can obtain high surface quality with less roughness. However, the grinding process consumes much larger energy in the process of material removal, and such high-energy input is almost completely dissipated as the heat, and leads to high temperatures in the grinding zone. As a result, the high temperature may damage the work-piece, such as the softening of the ground surface, the geometrical accuracy. As the same time, high temperatures affect process times and accelerate wear of the grinding wheel (Kinalkar *et al.*, 2014; Zhang *et al.*, 2013). The popular approach for holding grinding temperatures within appropriate limits is the use of liquid coolants. Liquid coolants decrease work-piece temperature and reduce the risk of thermal damage. However, despite their advantages, liquid coolants have some disadvantages which recommend limiting or even eliminating their use. The main disadvantages are economical costs, environmental effects and health hazard limitations (Babic *et al.*, 2005; Garcia *et al.*, 2013). And these factors caused a search for better cooling approaches which should satisfy the following conditions: to be effective, cheap and environment-friendly (Babic *et al.*, 2005). Mist/air jet flow impinged on grinding zone is considered as one of the promising cooling approaches to satisfy the above-mentioned condition, which is easily realized by mixing a little bit of liquid into the high-speed air flow (Zhang *et al.*, 2013). Nguyen *et al.* (2003) discussed the applicability of cold air and oil mist in the grinding zone, and their results showed that their cooling capacity is enhanced by help of the addition of very small amount of oil mist. Babic *et al.* (2005) preformed some experiments on the grinding process with a mist/air jet cooling by injecting a little bit of water into air flow, and their results showed the cooling effects of simple water in air mist jets applied to grinding are quite impressive. Zhang, *et al.* (2013) made an assessment of the quantitative evaluation for heat transfer enhancement on a grinding work-piece surface subjected to the mist/air jet impingement by experimental investigation, and the results showed that the mist/air ratio played an important role for affecting the temperature and heat transfer coefficient distributions.

Due to importance of mist/air jet flow cooling, lots of investigations are reported. Li *et al.* (2001a) observed a heat transfer enhancement owing to the mist be added to steam in an impingement flow, and they concluded that up to 200 percent heat transfer was enhanced at the stagnation point by injecting only 1.5 percent of mist. Then they (Li *et al.*, 2001b) proposed a model for heat transfer in mist/steam impinging jet. Chang *et al.* (2001) investigated the heat transfer of an impinging air-water mist jet, and the detailed heat transfer coefficient distributions of the mist jet impingement flows were obtained, which confirmed the heat transfer enhancement of impinging mist-jet. Li *et al.* (2003) made experiments to study mist/steam heat transfer with jet impingement onto a concave surface, and the results indicated that the cooling was enhanced significantly near the stagnation point. Wang *et al.* (2005) made experimental investigation for the mist/steam heat transfer of three rows of circular jet impingement in a confined channel, and the results indicated that the number of jet and the jet diameter had influences on the heat transfer enhancement. Xie *et al.* (2013) also conducted experiments to study the heat transfer effects of air-R134a (a refrigerant), and found that a relative heat transfer enhancement of 36% was under condition of mixture flow spraying to the macro-structured surface.

In the grinding process with air/mist jet flow, owing to the interaction between air/mist jet impingement and the swirl flow entrainment induced by the rotated grinding wheel, the vicinity of the grinding zone suffered their connected effect, which made the convective heat transfer on grinding work-piece surface more complexity. Some studies have been made for the heat transfer enhancement over rotating grinding wheel by jet impingement. Saniei *et al.* (2000) reported heat transfer results of a spinning wheel cooled with an impinging air jet directed on its free surface, and examined the effects of rotation (rotational Reynolds number, jet Reynolds number) and jet impingement (jet-to-disk spacing, the location of the jet center) on heat transfer. Ebbrell *et al.* (2000) studied the effect of nozzle position on the volume of cutting fluid passing beneath the grinding wheel, and an increased flow rate beneath the wheel was realized by raising the nozzle position above the area of reversed flow. Minagawa *et al.* (2004) conducted the detailed velocity measurement in the turbulent boundary layer of a rotating disk, and found that the effect of rotation is important in both the skew in the mean flow and in the centrifugal force. Due to the capability of simulating the cooling performance or temperature distribution under various operation conditions could provide quite useful guidelines to optimize the grinding efficiency, many works involved into the numerical simulation. Alberto *et al.* (2013) optimized the geometry of nozzle by using of the computational fluid dynamics (CFD) and finite element analysis (FEA). Zhou *et al.* (2013) established a three-dimensional finite element method to investigate the temperature distribution at different process parameters, and the results indicated that the grinding temperature predicted by simulation agreed well with the experiment data. Stefan *et al.* (2013) simulated the fluid flow and heat transfer in grinding process by means of CFD, and obtained the distribution of temperatures, pressures, velocities, and liquid volume fractions in and around the grinding region.

However, previous investigations paid little attention on the flow characteristic of two-phase in the vicinity of spinning grinding wheel, as well as the influences of the jet parameters. In present study, numerical simulation is performed to investigate the flow characteristics of mist/air jet impinges on a flat work-piece with a rotating grinding wheel mounted above the work-piece,

which the mist is as the discrete phase. Then the heat transfer model of mist/air is analyzed. Further, the influences of the number of jet nozzle, position, and nozzle diameter on heat transfer are discussed.

2. NUMERICAL APPROACH

2.1 Mathematical Model

A work-piece cooling process unites a discrete phase (water mist) and a continuous phase (air), therefore it is natural to use the DPM (discrete phase model) approach. The flow of the air phase was computed using volume-averaged Navier-Stokes equations (Salikov *et al.*, 2012):

$$\frac{\partial(\alpha_a\rho_a)}{\partial t}+\nabla\cdot(\alpha_a\rho_a\vec{v}_a)=0 \tag{1}$$

$$\begin{aligned}\frac{\partial(\alpha_a\rho_a\vec{v}_a)}{\partial t}+\nabla\cdot(\alpha_a\rho_a\vec{v}_a\vec{v}_a)&=-\alpha_a\nabla\cdot p_a\\ -\nabla\cdot(\alpha_a\vec{\vec{\tau}}_a)-\vec{S}_p+\alpha_a\rho_a\vec{g}&\end{aligned} \tag{2}$$

where, α_a, p_a, ρ_a and $\vec{v}_a$ are the volume fraction, pressure, density and velocity of air respectively; t is time; and g is the gravitational acceleration. The stress tensor $\vec{\vec{\tau}}_a$ and drag force sink term $\vec{S}_p$ are given by:

$$\vec{\vec{\tau}}_a=-(\lambda_a-\frac{2}{3}\mu_a)(\nabla\cdot\vec{v}_a)\vec{\vec{I}}-\mu_a((\nabla\vec{v}_a)+(\nabla\vec{v}_a)^T) \tag{3}$$

$$\vec{S}_p=\frac{1}{V_{cell}}\int_{V_{cell}}\sum_{i=0}^{N_p}\frac{V_i\eta}{1-\alpha_a}(\vec{v}_a-\vec{v}_i)D(\vec{r}-\vec{r}_i)dV \tag{4}$$

where, η is the interphase momentum transfer coefficient, r_i is the particle position, v_i denotes the velocity vector, μ_a is the dynamic viscosity of the air phase and V_i is the volume. In present study, the coefficient η is computed from the Ergun correlation (Eq. (5)) (Ergun, 1952) due to $\alpha<0.8$.

$$\frac{\eta d_p^2}{\mu_a}=150\frac{(1-\alpha_a)^2}{\alpha_a}+1.75(1-\alpha_a)\mathrm{Re} \tag{5}$$

where, Re is the particle Reynolds number, can be expressed as the following.

$$\mathrm{Re}=\frac{\alpha_a\rho_a|\vec{v}_a-\vec{v}_i|d_p}{\mu_a} \tag{6}$$

where d_p is particle diameter. The motion of a mist particle i is computed using Newton's second law and the Euler equation.

$$m_i\frac{d\vec{v}_i}{dt}=V_i\nabla p+\frac{V_i\eta}{1-\alpha}(\vec{v}_a-\vec{v}_i)+m_i\vec{g}+\sum\vec{F}_{c,i} \tag{7}$$

$$I_i\frac{d\vec{w}_i}{dt}=\sum\vec{T}_i \tag{8}$$

The terms on the right hand side of Eq. (7) are force owing to the pressure gradient, drag, gravity as well as the collision-induced particle-particle and particle-wall forces $\vec{F}_{c,i}$. $\vec{T}_i$ is the torque and I_i is the moment of inertia of the mist particle i.

The turbulence flow is modeled using a RNG $k-\varepsilon$ model with a standard wall function for near wall region. In many literatures (Salikov *et al.*, 2012; Zhu *et al.*, 1994; Sharif *et al.*, 2009; Tarpagkou *et al.*, 2013), the RNG $k-\varepsilon$ turbulent model David Tebera regard as one of the robust turbulence models for complex turbulent flows, and it can be described by Eqs. (9) and (10) respectively.

$$\begin{aligned}\frac{\partial(\alpha_a k_a)}{\partial t}+\nabla\cdot(\alpha_a\rho_a k\vec{v}_a)&=\nabla\cdot(\alpha_a a_k\mu_{eff}\nabla k_a)\\ +G_k+G_b-\rho\varepsilon&\end{aligned} \tag{9}$$

$$\begin{aligned}\frac{\partial(\alpha_a\varepsilon_a)}{\partial t}+\nabla\cdot(\alpha_a\rho_a\varepsilon_a\vec{v}_a)&=\nabla\cdot(\alpha_a a_\varepsilon\mu_{eff}\nabla\varepsilon_a)\\ +C_{1\varepsilon}\frac{\varepsilon_a}{k_a}(G_k+C_{3\varepsilon}G_b)-C_{2\varepsilon}\rho\frac{\varepsilon_a^2}{k_a}-R_\varepsilon&\end{aligned} \tag{10}$$

where G_k is the generation rate of turbulence kinetic energy due to mean velocity gradients, G_b is the generation rate of turbulence kinetic energy due to buoyance, a_k and a_ε are the inverse effective Prandtl numbers for k and ε respectively, μ_{eff} is the effective viscosity, $C_{1\varepsilon}$, $C_{2\varepsilon}$ and $C_{31\varepsilon}$ are turbulence model constants. The term R_ε in the equation accounts for the effects of rapid strain and streamline curvature which plays an important role in the anisotropy of the large-scale eddies (Ma *et al.*, 2000).

The energy equation in computational domain is given as the following (Mitra *et al.*, 2013).

$$\begin{aligned}\frac{\partial(\alpha_k\rho_k E_k)}{\partial t}+\nabla\cdot[\alpha_k\vec{v}_k(\rho_k E_k+p)]&\\ =\nabla\cdot(\lambda_k\nabla T_k)+S_h&\end{aligned} \tag{11}$$

where, k is either mist (water) or air; α_k, ρ_k, u_k, E_k, λ_k, and T_k are the volume fraction, the density, the velocity, the energy, thermal conductivity, and the temperature of the k-th phase respectively; p is pressure; and S_h is energy source term owing to heat transfer.

The local convective heat transfer coefficient h on the work-piece surface is evaluated as following.

$$h=\frac{Q-Q_s}{A(T_w-T_j)} \tag{12}$$

where T_w is the heated plate temperature on the top surface, T_j is the jet temperature, A is the effective area of heating foil, Q is the input power imposing on heating foil, and Q_s is the heat loss from heater

insulation.

2.2 Numerical Application

In order to verify in detail the proposed model, the previous laboratory experiments performed by Zhang *et al.*. (2013) are reproduced numerically, and the results are compared aiming to evaluate how realistic and reliable the numerical simulations of the proposed model are. The computational domain is shown in Fig. 1, which represents the fictitious grinding process of grinding wheel touching the work-piece. The work-piece is 500mm in length and 2mm in thickness, with the bottom surface subjected to uniform heat flux. The rotating wheel is 200mm in diameter. The central line of grinding wheel is located at the symmetry line of computational domain. Two coordinate systems are established, one is the stationary coordinate system with original point located at the center of wheel, and the other is rotational coordinate system with original point located at the center of wheel. The jet nozzle is located at a coordinate of (L=65mm, H=10mm) in the stationary coordinate system, with diameter of 5mm and inclination angle of 20° (β).

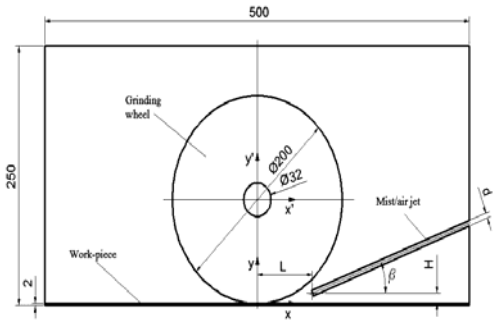

Fig. 1. Schematic of computational domain.

Due to solve the definition problem of the interface between rotating wheel and stationary work-piece for really grinding process whether the interface is in rotation or in stationary, A tiny gap (0.02mm) is set between the rotational grinding wheel and work-piece. Because the velocity of the work-piece moving is small relative to both the impinging jet and the grinding wheel tangential velocities, the work-piece is assumed as stationary.

Numerical simulations using commercial software (FLUENT 14.5) are conducted to understand the flow patterns and heat transfer in the vicinity of a rotating wheel with jet impingement directed at heating work-piece. The computational domains include the rotating wheel, stationary work-piece and surrounding fluid. The computational domain is meshed employing Workbench 14.5, and grids are refined in some critical regions to ensure coverage for satisfactory resolution, especially near the no-slip walls where velocity and temperature gradients are expected to be high. Based on the mesh independence test, 50566 cells and 53019 nodes are involved in the whole computational domain, and the meshed computational domain is shown in Fig. 2.

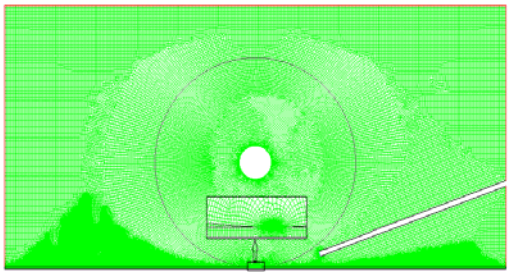

Fig. 2. meshed computational domain.

The SIMPLE scheme is selected for the pressure-velocity coupling, the standard for pressure and the two order upwind for the momentum, the turbulence energy and the specific dissipation. Convergence is considered achieved when the residuals of the different variables are lowered by four orders of magnitude.

The computational domain boundaries of are specified as the following.

1) The constant heat flux is specified at the bottom surface of work-piece with q=1000 W/m^2. The thermal conductivity of work-piece is 16 W/(m·K). The coupling thermal boundary is imposed on the top surface of work-piece.

2) The coupling thermal boundary is imposed on the edge surface of grinding wheel. The thermal conductivity of the grinding wheel is 0.1 W/(m·K). And a rotational angular speed (2000 rpm in anti-clockwise) is applied to the solid wheel.

3) At the impinging jet in initial computation, the uniform inlet velocity is 30 m/s and temperature is 300K. This inlet is set as the injection plane where the mists are released when the DPM is coupled.

4) The temperature on coupling interfaces is determined according to thermal equilibrium relationship. No-slip wall boundary conditions are employed for all solid surfaces. The fictitious boundaries of fluid domain are set as pressure-outlet boundary (0 Pa, 300K).

The coupling between the mist phase and the air phase medium is accomplished as follows. The equations for the air phase are solved prior to the injection of the mist. The equations for the water mist phase are then introduced, and the trajectories for the mists are computed. The effect of the discrete mists onto the air phase is then considered by resolving the air phase equations with the newly computed source terms associated with the presence of the mists. The mists trajectories are then recomputed based on the modified results of the air phase equations. The procedure is repeated until solution convergence is achieved.

3. RESULTS AND DISCUSSES

3.1 Validation of the Model with Experimental Results

Initially the numerical simulation is carried out to

compare the experimental data of Zhang *et al.* (2013), whose experimental setup includes the air pump, the water tank, the siphon nozzle, and the flow meter, the valve, the heater, the thermal couple, the motor disk, the data collection and the control system. The air and water were separately and precisely fed into the mixing chamber of siphon nozzle by the controllable valve. The corresponding mist/air ratio (F_w / F_a , F_w is the water volumetric flow rate while F_a is the air volumetric flow rate) is 1.412‰. Fig. 3 represents the simulated results and the experimental results of the heat transfer coefficient distributions over the top surface of work-piece. It is obvious that the simulation results agree well with the experimental data.

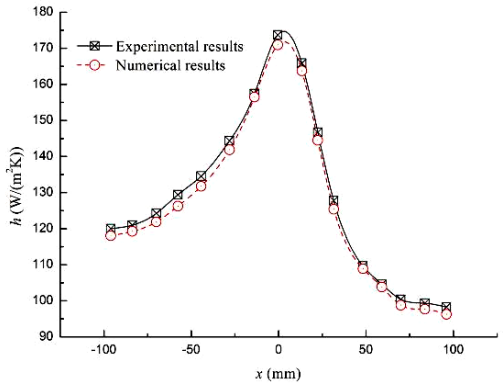

Fig. 3. Comparison of results in experiment and simulation.

3.2 Analysis of Flow Field and Mechanism of Heat Transfer

After validation with experiments, the model is used to generate additional information on the flow field of computational domain. Fig. 4 shows computational results of flow field induced by rotating grinding wheel and the mist/air jet, such as the pressure contour, velocity contour, temperature contour, velocity vector, streamline, and mist particle tracks in the computational domain. Fig. 4a depicts the pressure distribution during the grinding, and it indicates that the pressure is the highest in the area among of the mist/air inlet, the work-piece, and the grinding wheel. Due to be blocked by the grinding wheel and work-piece, the mist/air jet flow changes the flow direction sharply, which causes the pressure in this area to increase.

The velocity contour and vector are presented in Fig. 4b and 4c. It is noted that a rotating grinding wheel brings air from the surroundings and leads to a spiral fluid flow over the rotating wheel, and the predominant flow direction is tangential. In the negative x-direction, as the spiral air flow reaches the minimum gap between the wheel and the work-piece, some of the flow stagnates and then flows backwards away from the grinding zone. However, in the positive x-direction, the jet flow reaches the minimum gap, and is blocked by the grinding wheel and the work-piece, causes the recirculation flow. The tangential velocity of swirl flow near grinding zone is opposite to the impinging jet velocity, the

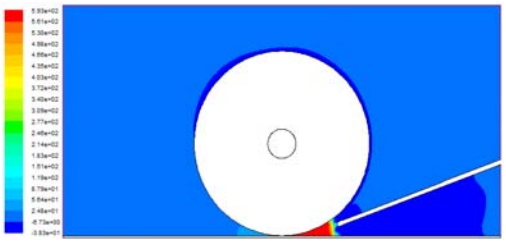

a) pressure contour

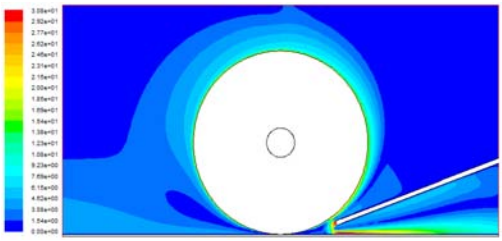

b) velocity contour

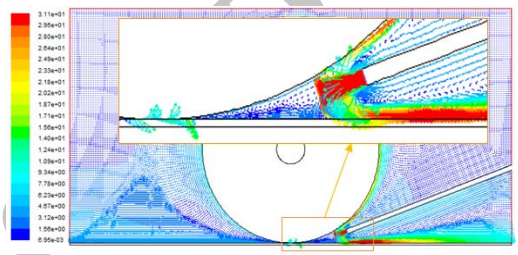

c) velocity vector

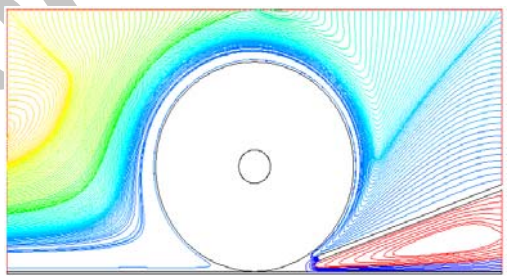

d) streamline

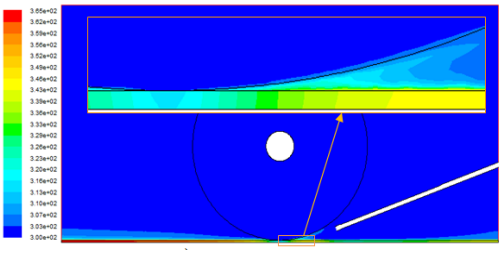

e) temperature contour

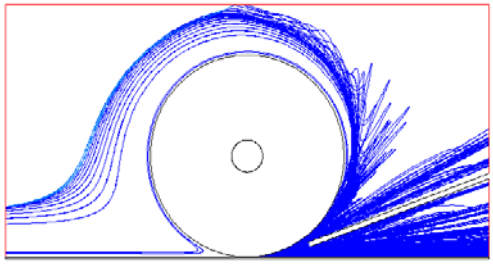

f) mist particle tracks

Fig. 4. Flow field of computational domain.

swirl flow comes into collision with the jet flow, and forms the stagnation zone, which the mixture flow changes sharply its direction. From Fig. 4b and 4c, the maximum velocities are located in a region of inlet jet and surface of work-piece under the jet nozzle.

Fig. 4d represents the streamline in the computational domain, and it further explains the flow situation in Fig. 4b and 4c. The streamlines have been divided two directions, one flows along the grinding wheel, and the other flows along the work-piece to form the recirculation flow.

Fig. 4e illustrates the temperature distribution in the computational domain, and the enlarged view is the temperature distribution of work-piece cross-section. The stagnation zone subjected to the impinging jet has the lowest temperature. This is because of coupled action of swirl flow and jet flow, the former is contributed to that the rotational effect of grinding wheel tends to push the mixture flow to the surface of work-piece, while the latter is contributed to that the jet flow blocked by wheel and then comes into with the heating surface of work-piece under the jet nozzle wedge.

The mist particle tracks are shown in Fig. 4f, it is obvious that the mist particles flow from the nozzle, and flow upward and downward due the block of the grinding wheel and the work-piece. The mist particles neared the grinding wheel flow along the profile of the wheel, and the outer particles (far from the grinding wheel) flow with random trajectory. The reason for this may be that the rotating wheel influences the mist particles flow. The mist particles flow to downward come to work-piece and to the right. The trajectory of mist particles can be influenced by the rotating speed of the grinding wheel, and is shown in Fig. 5. As the rotating speed increases, the mist particles have enough energy to flow with the grinding wheel, and more particles flow back to the right. This may be caused by the centrifugal force of the rotating wheel. However, the direction of rotating is a factor to influence the motion of mist particles. When the grinding wheel rotates clockwise, the mist particles hardly flow to the left of the work-piece.

From Fig.4f and Fig. 5, the mist particles accumulate in zone of the positive x-direction, and more the mist particle accumulation, lower temperature on the surface of work-piece. The possible reason is that high velocity direction sharp change makes more droplets hit the surface of the work-piece in positive x-direction, and bring away more heat.

The heat transfer coefficient distributions on the top surface of heated work-piece in case of single air jet and mist/air mixture jet are obtained from the computation, and are presented in Fig. 6. It is obvious that the heat transfer coefficient increases as using the mist/air mixture flow.

For the mist/air impinging jet enhancing cooling effectiveness, two-phase heat transfer includes particle dynamics, additional momentum and mass transfer induced by evaporation of liquid droplets

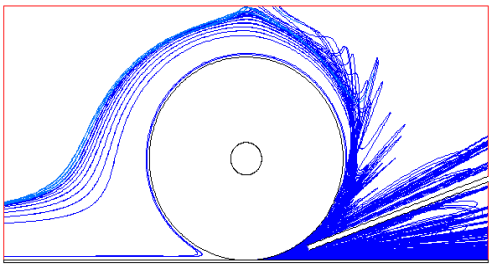

a) n=2000 rpm

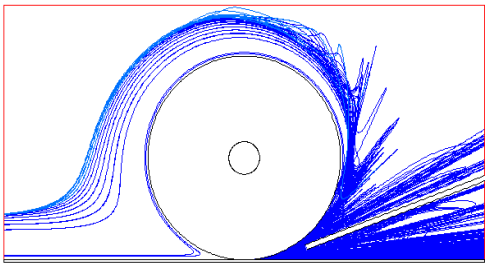

b) n=3000 rpm

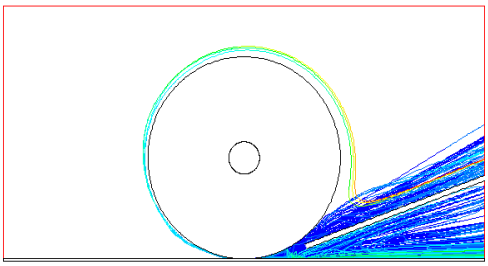

c) n=-2500 rpm

Fig. 5. Mist particle trajectory under different rotating speed of wheel.

on/near the heated surface, and increased specific heat, and the direct surface-to-droplet heat transfer during impact releasing the latent heat of evaporation. Therefore, the mixture of mist and air is introduced into the heat transfer system, and the mist (water) particles remove a part of heat from the surface of heated work-piece. According to the study of Li *et al.* (2001b), heat transfer between the droplets and air can be modeled by considering droplet as a distributed heat sink. The droplets evaporate into the superheated steam inside the thermal boundary layer and act to quench the boundary layer. Based on the superposition concept the temperature of mist/air flow is divided into two parts, $T = T_a + T_m$. T_a is the temperature of air-only flow and T_m is the temperature depression caused by the mist.

In the light of the two-dimensional energy equation, and by appropriately simplifying, the equations for T_a and T_m can be written as.

$$T_a = (T_w - T_{sat}) e^{-yh_o/k_s} + T_{sat} \tag{13}$$

$$T_m = \frac{\gamma^2 (T_w - T_{sat})}{\gamma^2 - (h_0 / k_s)^2} (e^{-\gamma y} - e^{-yh_o/k_s}) \tag{14}$$

where, γ is the coefficient, and

$\gamma = (12\alpha_{mist}\rho_a d_{10} / \rho_w d_{30}^3)^{0.5}$; α_{mist} is mist volume fraction; k_s is air heat conductivity; h_0 is air alone heat transfer coefficient; and y is coordinate perpendicular from the surface of work-piece.

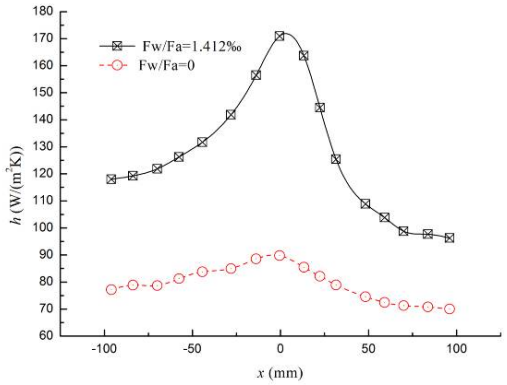

Fig. 6. Comparison of results in single-air jet and mist/air jet.

Therefore, the heat transfer increasing due to mist, h_2, defined as $-k_s(dT_m / dy)|_{y=0} /(T_w - T_{sat})$, can be written as following.

$$h_2 = \frac{h_0(\gamma k_s / h_0)^2}{\gamma k_s / h_0 + 1} \tag{15}$$

For the current study, in lieu of the experimental data $h_0 = 89.76$ W/m^{2}K, $\alpha_{mist} = 0.00141$, $\rho_a / \rho_w = 0.001212$, $k_s = 0.024$ W/mK, and $d_0 / d_{30}^3 = 1.4\times10^{12}$ m^{-2}, a value of $h_2 / h_0 = 0.845$ is obtained. This result is coincident with the experimental observation (Zhang *et al.*, 2013).

3.3 Analysis of Parametric Effects

The heat transfer performance is influenced by many factors, and Zhang *et al.* (2013) confirmed the heat transfer coefficient increased with increased rotational speed of grinding wheel and mist/air ratio. In present investigation, attempts have been made to understand the influence of the locations of jet nozzle, the diameter of jet nozzle, and the number of jet nozzle on the heat transfer coefficient.

In order to determine the effect of the locations of jet nozzle on the heat transfer coefficient, the jet nozzles located in the different x-direct position L, y-direction position H, and angle β are considered. The results are shown in Figs. 7-9. The effect of x-direct position L on heat transfer is presented in Fig. 7, and it is noted that heat transfer coefficient increases with decrease in L in the grinding zone (between x=-15 and x=20). The reason may be that as L increases, the jet nozzle is far away from the grinding zone, and leads to the cooling action decrease. On the left surface of grinding zone (x< -30), the heat transfer coefficient is not signification influenced by L. However, on the right surface of grinding zone (x>30), the heat transfer coefficient increases with increase in L, because the jet nozzle is relatively close to this zone as L increases.

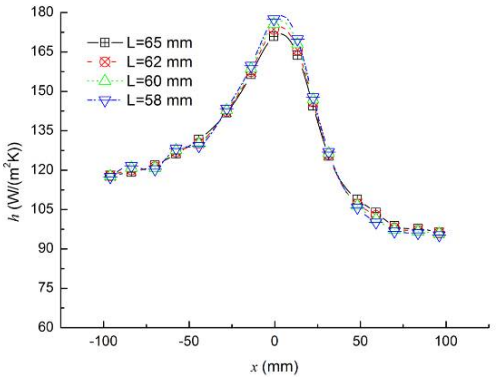

Fig. 7. Heat transfer coefficient distribution at different L.

Fig. 8 demonstrates the effect of y-direction position H on heat transfer. It is obvious that it is similar to heat transfer coefficient increases with decrease in H in the grinding zone (between x=-15 and x=20). On the left surface of grinding zone, the heat transfer coefficient is not obvious variation trend along H increasing. But on the right surface of grinding zone, the heat transfer coefficient increases with increase in H, because the jet flow cone radius of nozzle relatively increases with the increase of H, leads to the more areas acquire the mist/air flow.

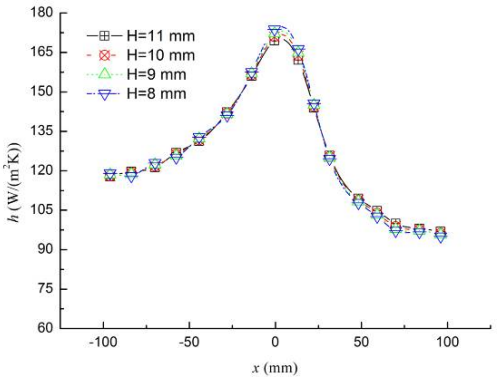

Fig. 8. Heat transfer coefficient distribution at different H.

Fig. 9 illustrates the effect of nozzle inclination angle (β) on heat transfer. For grinding zone and the right surface of grinding zone, the heat transfer coefficient increases with decrease in β. It is apparent that the jet flow is blocked by the rotating grinding wheel, and this is more severe for the larger β. And it similar to Figs. 6-7, on the left surface of grinding zone, the heat transfer coefficient alternating increase and decrease with increase in β.

In order to investigate the effect of jet nozzle position on heat transfer, three jet nozzle positions are considered, and are shown in Fig. 10a. The effect of jet nozzle position on heat transfer coefficient is represented in Fig. 10b. From this figure, as the distance of between jet nozzle and the

grinding zone increases, the heat transfer coefficient decreases obviously. This can be supported by the experimental investigation on single air jet cooling grinding zone (O'Donovan *et al.*, 2006) Fig.10c depicts the tracks of mist in case of jet nozzle in the middle position and the top position, while the track of mist in bottom position is shown in Fig.4f, and these tracks of mist help us to understand the variation of heat transfer coefficient. This figure also indicts that the mist particles trajectory could influence by the position of nozzle.

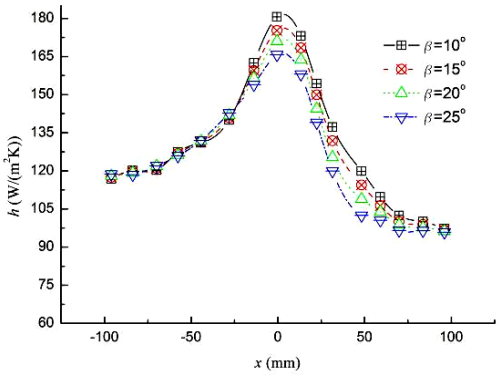

Fig. 9. Heat transfer coefficient distribution at different β.

In a further attempt to analyze the effect of nozzle diameter on heat transfer, four cases with different nozzle diameter are computed, and the heat transfer distributions are depicted in Fig. 11. It can be noticed that an increase in nozzle diameter induces to an increase in heat transfer. This is because the larger nozzle diameter generates more mist/air flow impacting to the grinding zone and the surface of work-piece, and contributes to the enhanced heat transfer.

Subsequently, an attempt has been performed to understand the influence of nozzle number on heat transfer. This is achieved by comparing the heat transfer under condition of one jet (see Fig.1) and two jets (see Fig. 12a), and the results are shown in Fig. 12b. It can be seen that heat transfer coefficient increases with an increase in nozzle number. And this figure also shows that the heat transfer coefficient has not obvious difference for the left and right of the grinding zone. The mist particle tracks are shown in Fig. 12c, it can help to explain the reason that the cooling effect is improved. Also, the trajectory of the mist particles is very different for comparing that under condition of the single nozzle.

4. CONCLUSIONS

The heat transfer on grinding work-piece with mist/air impinging jet has been simulated by using DPM model, the detailed flow and heat transfer characteristics in the computational zone neared the grinding zone are obtained, and the results are in good agreement to the experimental results. Further the mechanism of mist/air impinging jet to enhance cooling effectiveness, and the effect of jet nozzle location, nozzle diameter, and nozzle number on heat transfer are investigated.

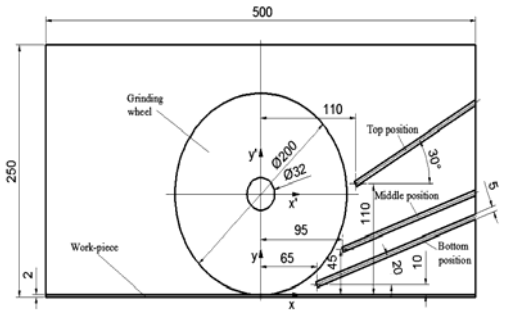

a) different jet positions

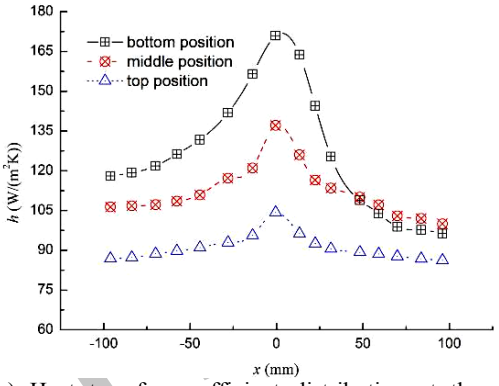

b) Heat transfer coefficient distribution at three different positions

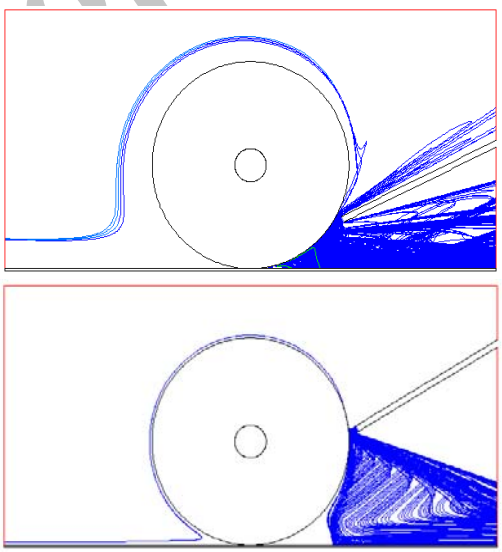

c) The track of mist particle in case of middle position and top position

Fig. 10. Heat transfer coefficient distribution at three different positions.

The results of DPM simulation shows the mist droplets (or particles) can be accumulated on the right surface of grinding zone, and the mist particles flow can be affected by the rotating speed of the grinding wheel, the position of nozzle, and the number of nozzle. The mechanism model of enhance cooling by mist/air impinging jet is developed, which indicates the mist droplet plays key role in enhancing mechanism, and the heat

transfer coefficient at grinding zone increases 84.5% by injecting 1.412 ‰ of mist.

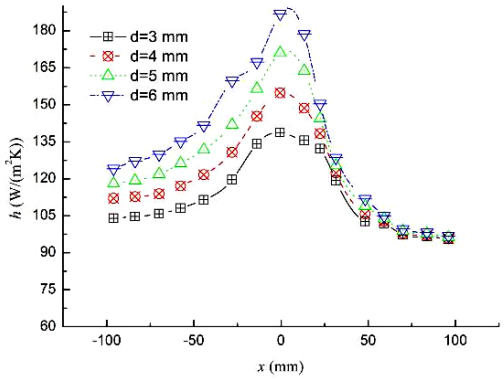

Fig. 11. Heat transfer coefficient distribution under different diameter of nozzle.

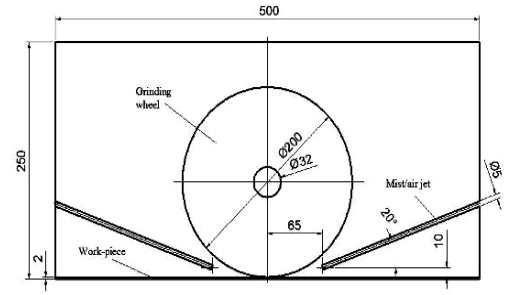

a) Two jets

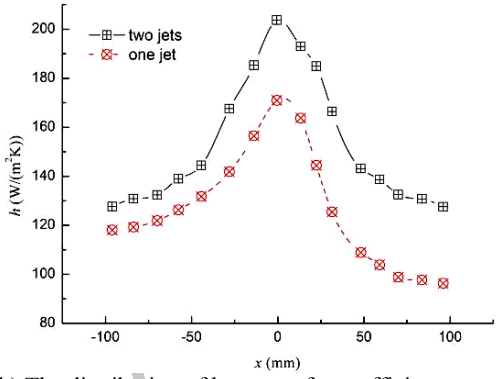

b) The distribution of heat transfer coefficient

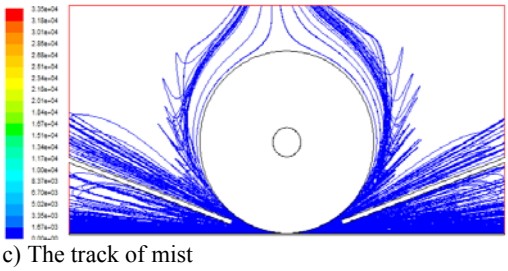

c) The track of mist

Fig. 12. Influence of nozzle number on heat transfer.

The heat transfer coefficient is influenced by the jet nozzle location, nozzle diameter and nozzle number. The jet nozzle is placed much nearer the grinding zone, causes greater the heat transfer coefficient. The heat transfer coefficient increases with decrease in β. An increase in nozzle diameter induces to an increase in heat transfer. The heat transfer coefficient increases with an increase in nozzle number.

ACKNOWLEDGEMENTS

The authors gratefully acknowledge the financial support for this project from the Open Fund of Guangdong Provincial Key Laboratory of Micro-nano Manufacturing Technology and Equipment (grant no. GDMNML2013-02).

REFERENCES

Alberto, L. A., C. German, N. D. Hom and A. Raul (2013). High performance composite nozzle for the improvement of cooling in grinding machine tools. *Composites: Part* B 54, 313-318.

Babic, D., D. B. Murray and A. A. Torrance (2005). Mist jet cooling of grinding processes. *International Journal of Machine Tools and Manufacture 45*, 1171-1177.

Chang, S. W. and L. M. Su (2001). Heat transfer of confined impinging air-water mist jet. *JSME International Journal Series B* 44, 274-287.

Ebbrell, S., N. H. Woolley, Y. D. Tridimas, D. R. Allanson and W. B. Rowe (2000). The effects of cutting fluid application methods on the grinding process. *International Journal of Machine Tools and Manufacture* 40, 209-223.

Ergun, S. (1952). Fluid flow through packed columns. *Chemical Engineering Progress* 48, 89-94.

Garcia, E., Pombo, I., Sanchez, J. A., Ortega, N., Izquierdo, B., Plaza, S., Marquinez, J. I., Heinzel, C.,

Kinalkar, R. B. and M. S. Harne (2014). A review on various cooling system employed in grinding. *International Journal of Innovative Technology and Exploring Engineering* 4, 28-35.

Li, X., J. L. Gaddis and T. Wang (2001). Mist/steam heat transfer in confined slot jet impingement. *ASME Journal Turbomachines* 123, 161-167.

Li, X., J. L. Gaddis and T. Wang (2003). Mist/steam heat transfer with jet impingement onto a concave surface. *ASME Journal of Heat Transfer* 125, 438-446.

Li, X., J. L. Gaddis and T. Wang, (2001). Modeling of heat transfer in a mist/steam impingement jet. *ASME Journal of Heat Transfer* 123, 1086-1092.

Ma, L., H. D. B. Inghamst and X. Wens (2000). Numerical modelling of the fluid and particle penetration through small sampling cyclones. *Journal Aerosol Science* 31, 1097-1119.

Minagawa, Y. and S. Obi (2004). Development of turbulent impinging jet on a rotating disk. *International Journal of Heat and Fluid Flow* 25, 759-766.

Mitra, S., M. J. Sathe, E. Doroodchi, R. Utikar, M. K. Shah, V. Pareek, J. B. Joshi and G. M. Evans (2013). Droplet impact dynamics on a spherical particle. *Chemical Engineering Science* 100, 105-119.

Mourek, D. (2013). Reduction of oil and gas consumption in grinding technology using high pour-point lubricants. *Journal of Cleaner Production* 51, 99-108.

Nguyen, T. and L. C. Zhang (2003). An assessment of the applicability of cold air and oil mist in surface grinding. *Journal of Materials Processing Technology* 140, 224-230.

O'Donovan, T. S., D. B. Murray and A. A. Torrance (2006). Jet heat transfer in the vicinity of a rotating grinding wheel. *Proceedings of the Institution of Mechanical Engineers, Part C: Journal of Mechanical Engineering Science* 220, 837-845.

Salikov, V., S. Antonyuk and S. Heinrich (2012). Using DPM on the way to tailored prismatic spouted bends. *Chemie Ingeieur Technik* 84, 388-394.

Saniei, N. and X. Yan (2000). An experimental study of heat transfer from a disk rotating in an infinite environment including heat transfer enhancement by jet impingement cooling. *Journal of Enhanced Heat Transfer* 7, 231-245.

Sharif, M. and K. K. Mothe (2009). Evaluation of turbulence models in the prediction of heat transfer due to slot jet impingement on plane and concave surfaces. *Numerical Heat Transfer, Part B: Fundamentals* 55, 273-294.

Stefan, D. M., C. Sorin and D. M. Ioan (2013). Detailed study of fluid flow and heat transfer in the abrasive grinding contact using computational fluid dynamics methods. *Journal of Manufacturing Science and Engineering* 135, 041002.

Tarpagkou, R. and A. Pantokratoras (2013). CFD methodology for sedimentation tanks: The effect of secondary phase on fluid phase using DPM coupled calculations. *Applied Mathematical Modelling* 37, 3478-3494.

Wang, T., J. L. Gaddis and X. Li (2005). Mist/steam heat transfer of multiple rows of impinging jets. *International Journal of Heat and Mass Transfer* 48, 5179-5191.

Xie, J. L., Y. B. Tan, F. Duan, K. Ranjith, T. N. Wong and K. C. Toh (2013). Study of heat transfer enhancement for structured surfaces in spray cooling. *Applied Thermal Engineering* 59, 464-472.

Zhang, J. Z., X. M. Tan, B. Liu and X. D. Zhu (2013). Investigation for convective heat transfer on grinding work-piece surface subjected to an impinging jet. *Applied Thermal Engineering* 51, 653-661.

Zhou, L., S. T. Huang and C. Y. Zhang (2013). Numerical and experimental studies on the temperature field in precision grinding of SiCp/Al composites. *International Journal of Advanced Manufacture Technology* 67, 1007-1014.

Zhu, J. and T. H. Shih (1994). Computation of confined co-flow jets with three turbulence models. *International Journal for Numerical Methods in Fluids* 19, 939-956.